

Automated defect detection for ultrasonic inspection of CFRP aircraft components[☆]

Loïc Séguin-Charbonneau^{a,*}, Julien Walter^a, Louis-Daniel Théroux^a, Laurent Scheed^a, Alexandre Beausoleil^a, Benoit Masson^b

^a Centre technologique en aérospatiale, 5555 Rue de L'ÉNA, Saint-Hubert, QC, J3Y 8Y9, Canada

^b Bombardier Aviation, 1800 Boul. Marcel-Laurin, Saint-Laurent, QC, H4R 1K2, Canada



ARTICLE INFO

Keywords:
Ultrasonics
Algorithm
Composite materials
Reconstruction
Signal processing

ABSTRACT

An automated task sequence based on the commercial software Ultis® combined with new pre- and post-processing tools was developed to achieve a fully automated analysis of ultrasonic data obtained from large and complex CFRP components. The resulting $a_{90/95}$ on reference panels containing a variety of artificial defects was 6.8 mm. The new tools include a C-scan projection optimizer that minimizes defects distortion during 3D to 2D transition, an efficient segmentation method to address challenging features (co-cured stringers, ply drop-offs, multiple thickness variations), and a novel defect detection algorithm capable of automatically extracting indications from a collection of A-scans. Results suggest that the method meets the detection requirements while significantly reducing the analysis time.

1. Introduction

1.1. Background

Polymer matrix composites are extensively used in the design of modern aircrafts primary structures. Their specific strength allows for significant weight savings. Structural components made of carbon fiber reinforced polymers (CFRP) must be 100% inspected to detect potential manufacturing flaws such as delamination, porosities or inclusions. Ultrasonic testing (UT) is the preferred method for the inspection of CFRP laminates, due to its efficiency and reliability [1].

UT scanning operations used in production are nowadays widely automated, by means of large gantries, immersion tanks or robotized systems [2]. This equipment allows for fast scanning speed with high spatial resolution which generates tremendous amount of data. Most recent aircrafts can have several tens of square meters to be inspected with a typical scanning resolution of 1–2 mm. However, data analysis

and interpretation are still generally performed by human operators which is time-consuming, costly, requires highly trained personnel and may create bottlenecks in the manufacturing process [3].

In this context, automated analysis is increasingly used in the aerospace industry for a more efficient processing of such large amount of data. Major time savings and reliability improvements can be expected from these approaches. However, their application on large and complex CFRP structures in a context of production still faces numerous challenges: analysis of 3D parts with 2D tools and criteria, defect detection in difficult areas such as steep thickness variations, complex geometric features or near the interfaces.

1.2. Prior work

Automated analysis of ultrasonic data has been an active research topic in academy and industry since the 1980's. Aldrin et al. [3] list numerous techniques that have been developed and adapted for automatic detection

* This work was supported by the Natural Sciences and Engineering Research Council of Canada (NSERC), Fonds de recherche du Québec - Nature et technologies (FRQNT), Bombardier Aviation and the Programme d'aide à la diffusion des résultats de recherche au collégial (PADRRC) of Québec's Ministère de l'Enseignement supérieur (MES).

* Corresponding author.

E-mail addresses: l.seguin-charbonneau@cegepmontpetit.ca (L. Séguin-Charbonneau), julien.walter@cegepmontpetit.ca (J. Walter), louis-daniel.theroux@cegepmontpetit.ca (L.-D. Théroux), laurent.scheid@cegepmontpetit.ca (L. Scheed), alexandre.beausoleil@cegepmontpetit.ca (A. Beausoleil), Benoit.Masson@aero.bombardier.com (B. Masson).

URL: <https://www.cegepmontpetit.ca/cta> (L. Séguin-Charbonneau).

and classification of defects in composite materials such as image enhancement, image segmentation, pattern recognition or advanced signal processing techniques.

Several authors specifically focused on the automated analysis of ultrasonic C-scans. For example, Mahmud et al. [4] propose a simple method of flaw detection by applying a threshold on C-scan images. Goodfriend [5] and Smith et al. [6] compare the inspection data to reference C-scans obtained from ultrasonic simulations or from prior inspections of parts considered sound. Flaws are detected by subtracting the reference C-scan from the inspected C-scan. To make this comparison, an alignment of both images is necessary. However, it is difficult to get a perfect alignment for large parts which might lead to an important rate of false calls. Pérez et al. [7] propose a similar method in which the inspector manually defines the different homogeneous parts of the C-scan and chooses a detection threshold to be applied. This method still largely relies on the inspector skills.

Simas Filho et al. [8] propose a decision system to support the automatic inspection of fiber-metal laminates. Their method consists in detecting defects through neural networks applied to the frequency content of A-scan signals. However, this method relies on full RF signals that are not always available in a production context. In the aerospace industry, A-scan signals are often either strongly compressed or simply unsaved in order to limit the size of data files.

Aldrin et al. [3] suggest a global method for automatic C-scan data detection implemented in a software used by the Air Force Research Laboratory. The developed method is designed to adapt to the thickness of inspected parts. A time-spatial signal processing technique is also used to improve flaws detection close to the parts boundaries. Aldrin et al. note that the developed algorithm could be improved for detection near the backwall.

Barut and Dominguez [9] describe the automated analysis tool included in NDT kit® software (or its commercial version Ultis®). The method implemented in Ultis® uses a tool called *Backwall Echo Filter* (BWEF) which allows extracting indications from a time of flight (ToF) C-scan. This tool divides the C-scan image by automatically grouping pixels with similar depths (using a threshold on standard deviation or local gradient) and then removes partitions having greater depth than the neighboring ones. The aim is to suppress all pixels corresponding to the backwall and to only keep intermediate echoes. This method gives good results for large CFRP components provided that the part has no steep thickness variation and that the defects are not too close to the backwall surface (otherwise defects are either suppressed by the BWEF if its threshold is too high, or false calls are generated if its threshold is too low).

Another detection method based on the subtraction of reference C-scans is also available in Ultis® but suffers from the same cited limitations linked to difficulties to get a proper alignment.

1.3. Objectives

The targeted components are the rear pressure bulkhead and the aft fuselage skins of a passenger aircraft. The rear pressure bulkhead is a large monolithic composite part. Its external diameter is about 3 m, which represents more than 7 m² to inspect with a scanning resolution of 1 mm². Also, it is a 3D complex part with multiple curvatures and ply drop-offs (Fig. 1). The aft fuselage is an assembly of skins which are large curved monolithic parts of approximately 3 m long including numerous thickness variations and reinforced by co-cured stringers (Fig. 2).

The objective of this study is to develop an automated analysis method applicable to complex components with the following constraints and requirements:

1. The processing should be fully automated (little or no human intervention)

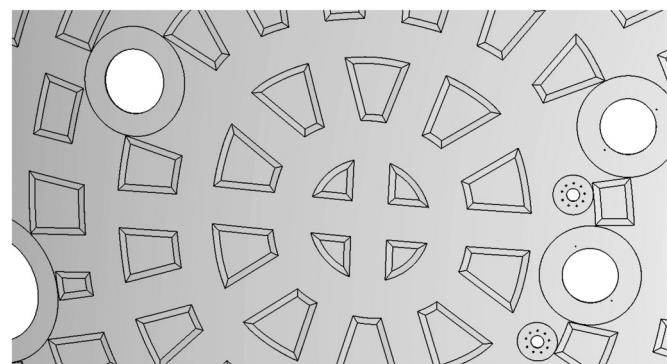


Fig. 1. Partial view of the pressure bulkhead structure, showing areas with different thicknesses and multiple holes.

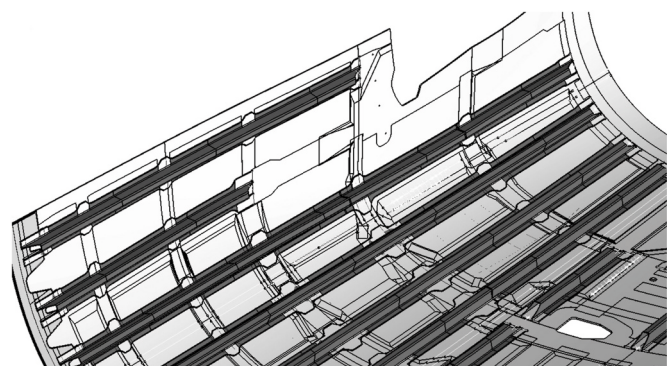


Fig. 2. Partial view of a fuselage skin, showing areas of multiple thicknesses and presence of co-cured stringers.

2. Components must be analyzed in their entirety, considering all their complexity (multiple curvatures, thickness variations, ply drop-offs, co-cured stringers, edges)
3. Input data is 3D but analysis must be done in 2D
4. Defects must be detected from the first to the last composite ply, for a particularly low ply thickness (approximately 0.150 mm)
5. Recorded A-scans are strongly compressed (using ALOK algorithm [10]).

2. Methods

2.1. General description of the steps

A method based on Ultis® existing modules and complemented by different pre- and post-processing tools was developed to comply with the above requirements. Three types of analysis are performed: thickness measurement, porosity assessment and defect detection. Various challenges were encountered during the design of this method.

First, the input data is acquired in 3D by the industrial gantry system, but most of the criteria and associated analysis tools in Ultis® are in 2D. Projecting the original 3D data to 2D without creating distortions that might impair defect detection, sizing or location is the first issue to address. An optimization routine developed to determine the best projection directions is described in Section 2.2.

Once the UT data is projected to 2D coordinates, several C-scans (ToF and amplitude) are generated with a set of different gates, each being optimized for a specific analysis. Various preprocessing steps are applied to those C-scans, such as pixels filtering to eliminate invalid data and correction of the backlash generated by the gantry system. Thickness measurement is first performed on the ToF C-scans. The following step is the porosity assessment, using both the ToF and amplitude C-scans (with

an average filter for the amplitude). The porosity criterion takes into account the additional attenuation caused by ply drop-offs or by the presence of additional copper mesh and/or glass ply layers on the parts surface.

The next step is the defect detection. It requires splitting the C-scans into segments consistent with the different geometric features or sub-structures. Achieving an efficient segmentation of complex parts is the second main challenge. A segmentation method, detailed in Section 2.3, was proposed to address this problem.

Once the C-scans are segmented, Ultis' *Back Wall Echo Filter* (BWEF) is applied on ToF C-scans to delete every pixel considered by the algorithm as a backwall echo, leaving only pixels containing intermediate echoes i.e., potential indications. The algorithm gives good results for defects located near the inspected surface or inside the part's volume but may not be adapted to detect defects too close to the backwall or located in areas where steep thickness variations occur. A new algorithm designed to get better results near the backwall surface was thus developed to complement the BWEF [11]. This algorithm is described in Section 2.4.

Once the backwall echo is filtered, defect detection is performed on the remaining indications using Ultis® dedicated tool. The criteria used are based on the length, width, areas and pixel densities of the remaining indications. Afterwards, defects that are close to each other or close to the edges are automatically grouped. Each defect or defect group is given a unique identifier and is then listed in a table indicating its position in 3D coordinates to be easily located on the actual part. Finally, the program automatically generates a report that includes data analyses and defect tables with screenshots of the indications. Details on the approaches developed within or in complement to Ultis® software are given in the next sections.

2.2. Projection optimizer

Ultis® is only able to perform the automated analysis of ultrasonic data on a flat two dimensional grid. To convert the three dimensional coordinates of the inspected part into a two dimensional coordinate system, the user defines rectangular prisms called *cuboids*. The segments of the inspected part contained inside each cuboid are orthogonally projected onto the corresponding cuboid face. An optimization routine was developed to select the best set of cuboids for a given part. Since the ultrasonic data is used to detect and size the defects, the objective function is to minimize the maximum local area distortion caused by the orthogonal projections.

Local area distortion is defined as follows. Assuming the part is a two dimensional manifold, a small enough region around each point will be planar. Consider a small circle tangent at a point with unit normal \mathbf{n} and area dA . If this circle is orthogonally projected onto a plane with unit normal \mathbf{N} , it becomes an ellipse of area $\mathbf{n} \cdot \mathbf{N} dA$. The local area distortion at the point is defined as the absolute value of the relative change in area caused by the projection:

$$\left| \frac{dA - \mathbf{n} \cdot \mathbf{N} dA}{dA} \right| = |1 - \mathbf{n} \cdot \mathbf{N}|$$

In order to evaluate the local area distortion, normal vectors at different points on the surface are required. A point cloud can be extracted from the CAD of the part. Ideally, this point cloud should cover the whole part as uniformly as possible. The surface normal at a point is taken to be the plane normal of a best fit plane through a small neighborhood of that point. Computation is done using the singular value decomposition of the centered coordinates matrix of the points in the neighborhood [12].

The optimization procedure finds the directions normal to the projection plane that minimizes the maximum local area distortion. An initial set of cuboids is provided by the user. From this set of plane normals, each point is assigned to the plane with the smallest local area

distortion. Powell's conjugate direction method [13] is used to minimize the maximum local area distortion over all points. Note that the assignment of points to planes might change at each iteration since the plane normals change.

A maximum number of cuboids was defined for each part in order to keep an acceptable trade-off between distortion and the number of C-scans to analyze. Fig. 3a shows an initial set of five cuboids defined by the user for a portion of the aft fuselage. The distortion at every point in each cuboid is shown in Fig. 3b. Fig. 3c shows the optimal set of cuboids along with the corresponding distortions (Fig. 3d). The maximum local area distortion decreased from 8.8% to 5.5% and the mean distortion decreased from 2.2% to 2.0%. Similar results were obtained for the bulkhead considered in this study, where a maximum local distortion of 5.95% was achieved.

2.3. Segmentation method

Barut and Dominguez [9] point out that a ToF variation below the threshold value set for the BWEF will be considered by the algorithm as a normal thickness variation, whereas abrupt thickness changes will be identified as potential defects. However, complex aircraft components such as the rear pressure bulkhead or the aft fuselage skins shown above include many ToF variations or spurious data in regions such as ply drop-offs, stringers or part edges. These areas might be falsely identified as defects if the BWEF is applied on the complete components and thus need to be analyzed separately. Two different approaches can be used to segment the C-scans and isolate areas containing similar structural or geometric features.

The most convenient elements to isolate on the aft fuse skins are the stringers which have clear boundaries on the ToF C-scans and can thus be easily identified by an automated process. A complete C-scan containing the stringers only can be reconstructed. This C-scan can be later analyzed separately from the skins with the defect detection tools (Fig. 4).

Furthermore, the part edges contain numerous spurious data that must be removed before defect detection, but these erroneous pixels make it difficult to clearly define the part boundaries. The chosen solution is to use masks with predefined shapes and locations.

However, while all inspected parts are theoretically identical, they are often slightly shifted from one another. An offset in rotation or translation is expected when installing the part on the inspection jig. This offset value was found to be in the range of 5–10 mm, which is normal for large parts such as the pressure bulkhead or the aft fuselage but represents a major issue when predefined masks with fixed positions are applied on the C-scans. Such masks cannot perfectly match the structural elements causing either false positives or loss of significant data.

In manual analysis, the operator could either correct each mask position individually, or align the overall C-scan. This alignment can be

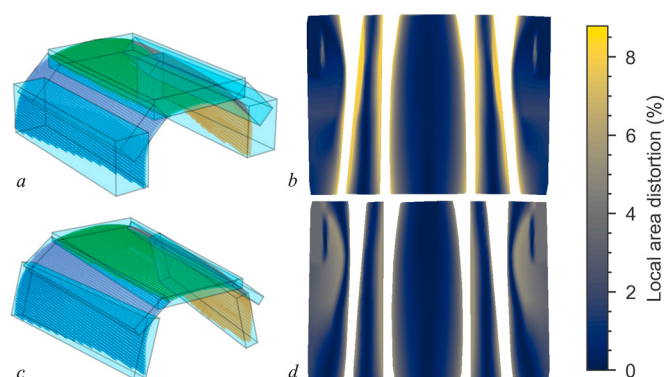


Fig. 3. Projection optimization for a fuselage portion.

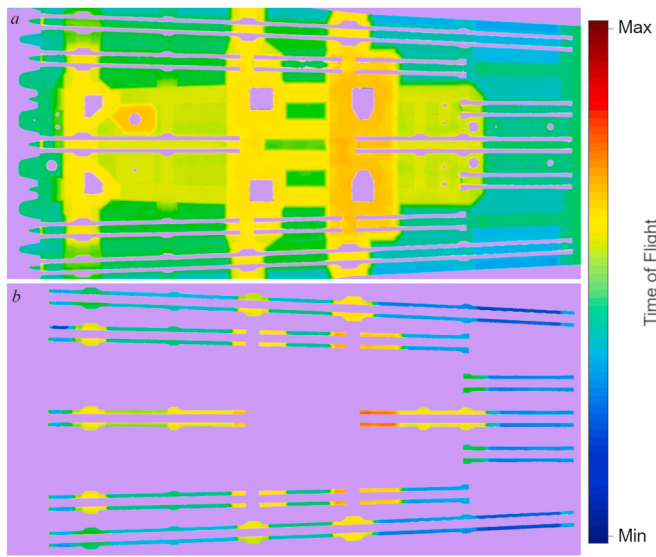


Fig. 4. Example of segmentation for a portion of the aft fuselage skin: skin (a) and stringers (b) can be isolated on different C-scans.

automated by using one single reference C-scan on which every acquired C-scans will be aligned. The alignment function must be based on a few specific geometric features. As the stringers are already isolated, the solution proposed is to use them to align each C-scan on the reference initially used to create the masks. Rotations and translations are automatically applied to the C-scan to align the stringers with their reference position. When the masks are loaded, they are thus well-positioned over the edges.

For the rear pressure bulkhead, there is no stringer or other similar structural element to rely on for a precise alignment of the masks. However, the holes for fluid passages and the edges contain numerous spurious pixels and should therefore be deleted before the analysis. The solution consists of taking advantage of the erroneous pixels in the edges' areas since they generally have ToF values outside of the part's thickness range. Most of the spurious pixels are filtered that way. In addition, every neighboring pixel is also filtered to obtain "clean" edges. Fig. 5 illustrates this process for a hole.

Finally, the rest of the holes can be removed using static masks significantly smaller than holes diameter. Thus, even if the C-scans are misaligned, the mask will not cause false positive or delete valid pixels. Some data is still deleted in the edges' vicinity with this method, but it was verified that the deleted areas are always smaller than the detection criterion.

Once the spurious data of the edges and holes are deleted, the C-scans of the bulkhead can then be segmented using masks isolating areas of similar thicknesses. A segment is created for each thickness plus a specific segment containing the ply drop-off areas only. Overlaps are set

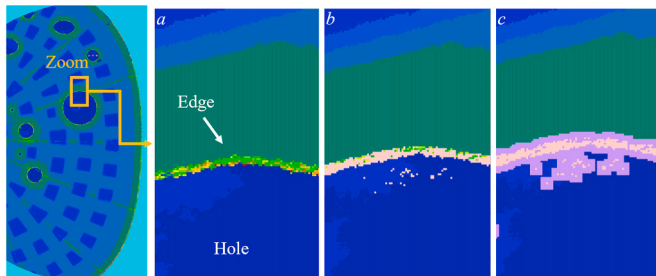


Fig. 5. ToF C-scan of a section of the bulkhead. In (a), some of the edge pixels have erroneous values. In (b), these pixels are filtered. In (c), the neighboring pixels are deleted to remove remaining pixels belonging to the edge.

between the segments to achieve a full coverage and to ensure that defects close to each segment's boundaries are detected.

2.4. New detection algorithm

A new detection algorithm was developed to take each part peculiarities into account and to give better results for defects close to the backwall surface [11]. The main concept consists in the subtraction of a reference C-scan that is automatically reconstructed from the data of each inspected part. The algorithm works in four main steps. 1) "Relevant" echoes are automatically extracted from each A-scan. 2) A matrix of backwall positions is computed based on the relevant echoes. A reconstructed backwall is then obtained by smoothing positions of the last echoes using cubic splines. 3) Reference envelopes are computed for front and backwall echoes using a statistical approach. Different envelopes are calculated for the different regions of the part to account for the local signal characteristics caused by geometric and lay-up configurations. 4) Calculated reference envelopes are subtracted from the recorded A-scans and a C-scan of remaining indications is finally computed. More details on these 4 steps are given in the following sections.

2.4.1. Identification of the relevant echoes

The method to identify front and backwall echoes is suitable for A-scans processed using the ALOK algorithm [10] and may require substantial modifications if a different data reduction technique was used. The front wall echo is simply defined as the echo with the smallest time of flight. The other echoes present on the A-scan can either correspond to defects, backwall or their respective repetitions. A backwall echo usually has a higher amplitude than all preceding echoes (except for the front wall echo) and should not occur at a time that is a multiple of the preceding echoes (otherwise it is a repetition). Using these criteria, a "last relevant echo" is automatically identified in each A-scan. The last relevant echo might correspond to a defect rather than the actual backwall. Indeed, some defects can reflect enough energy to make the backwall echo too faint to be identified correctly. This is the reason why the smoothing procedure described in the next section is necessary.

2.4.2. Reference backwall reconstruction

Each A-scan in the A-scan matrix has an (x, y) position and a time of flight associated to its last relevant echo, t . These triplets (x, y, t) form a three-dimensional point cloud approximating the position of the part backwall. If an A-scan contains a defect, the time of flight of the last relevant echo might be different from the actual position of the backwall. Smoothing the approximate backwall will eliminate defects and noise while maintaining an accurate representation of the real part backwall. The smoothing algorithm is based on two assumptions: 1) a defect area must be smaller than typical areas of thickness variations or surface deformations; 2) thickness variations or surface deformations of the real part backwall must be smooth in the mathematical sense (i.e., the backwall must be, to a good approximation, a smooth manifold).

Univariate cubic splines are used for smoothing the approximate backwall [14]. Even though bivariate splines could be used directly, they pose a computational problem on large surfaces since the memory requirements for computing bivariate splines with millions of data points is often prohibitive. A smoothing spline is computed at each fixed x_i and each fixed y_j . These splines define a grid over the A-scan matrix. Since the backwall curvature should be relatively smooth, the derivative of the splines should vary slowly and neighboring splines should have similar values.

Using sliding window statistics, points identified as outliers are removed from the approximate backwall and new splines are computed with the remaining points. After a few iterations (usually three to six), incorrect last relevant echoes are removed while maintaining a good fit even on regions where thickness varies (ply drop-offs, for instance). Fig. 6 shows an example of the spline smoothing process in a region

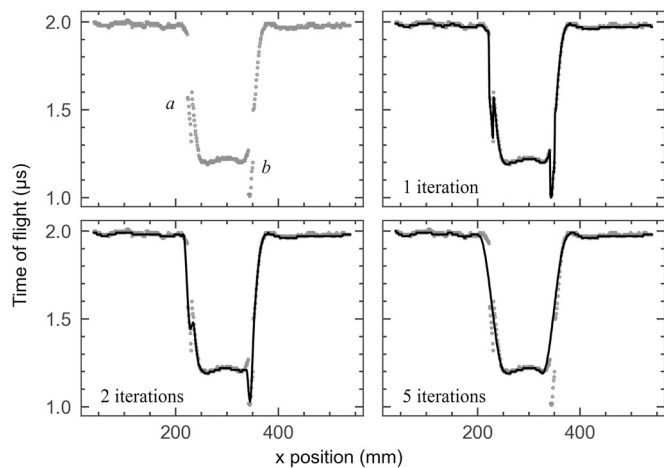


Fig. 6. Spline fitting process applied in a region including two ply drop-offs and two artificial defects (noted *a* and *b*).

containing two artificial defects *a* and *b* located in ply drop-offs. Grey points are the ToF of “last relevant echoes” obtained at the previous step. The black lines show the spline after different iterations of the process. After 5 iterations, a spline is obtained that follows the variations due to thickness changes, but excludes abrupt ToF variations due to defects *a* and *b*.

The final reconstructed backwall is obtained by averaging the two splines crossing at each point of the A-scan matrix and interpolating missing values using a simple bivariate linear interpolation. Fig. 7 shows an example of reconstructed backwall for a portion of the bulkhead.

2.4.3. Reference envelopes

Reference envelopes are constructed for both the front and back walls based on the echoes identified in the first step. For the backwall envelope, all last relevant echoes are superimposed (i.e., time-shifted in such a way that their maximum amplitude occurs at the same time of flight, see Fig. 8a). The reference envelope amplitude for a given peak is the *p*th percentile of all amplitude values superimposed at this time of flight (Fig. 8b). Choosing a high *p* (usually above 99) leads to an envelope that outlines the signals corresponding to the actual backwall while avoiding echoes caused by internal discontinuities. A Gaussian envelope is finally applied on each peak (Fig. 8c). A second reference envelope is constructed in the same way for the front wall echo. A set of specific reference envelopes is defined for each region depending on its lay-up configuration (for instance, ply drop-offs or flat regions, presence of outer layers such as glass ply or copper mesh, etc.).

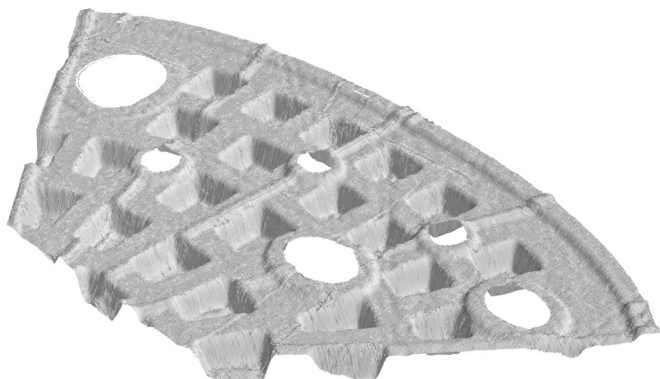


Fig. 7. Reference C-scan of a section of the rear pressure bulkhead reconstructed from measured data.

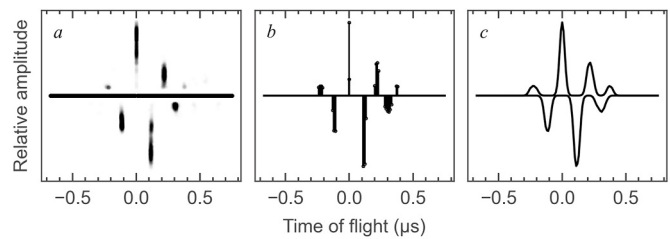


Fig. 8. Reference envelope calculation by superimposition of echoes (a), computation of a high percentile of each peak (b), and creation of an outline (c).

2.4.4. Subtraction and final filtering

For each A-scan position, the front reference envelope is shifted over the front wall echo to maximize cross-correlation between the two signals. The back reference envelope is shifted to the reconstructed backwall position. To compensate for noise and small discrepancies in the reconstructed backwall, the back reference echo can be further shifted by a small amount (less than half a period) to maximize cross-correlation.

A new A-scan is obtained by subtracting the shifted reference envelopes from the original A-scan. A low amplitude threshold is then applied to the resulting signal to suppress all non-significant peaks. At this stage, remaining peaks should correspond to indications.

Fig. 9 shows an example of subtraction of the reference envelopes. An indication is present on the ToF C-scan at the cursor position (Fig. 9a). On the A-scan corresponding to this pixel (Fig. 9b), the measured signal (vertical peaks) is not completely included in the reference envelope near the backwall echo. Consequently, some signal remains after the subtraction (Fig. 9c) and will be detected as an indication.

C-scans obtained with Ultis® BWEF and from the new detection algorithm can be combined by computing their binary addition. In the combined C-scan, a pixel is marked as an indication if either one (or both) of the two C-scans identified this pixel as an indication. This new combined C-scan can then be analyzed using Ultis® defect detection tool.

3. Experimental setups

For the rear pressure bulkhead (noted RPB from this point), a set of 5 flat test panels including artificial defects as well as 13 actual bulkheads were used to assess the performance of the developed method. The test specimens are monolithic unidirectional CFRP panels with 6 different

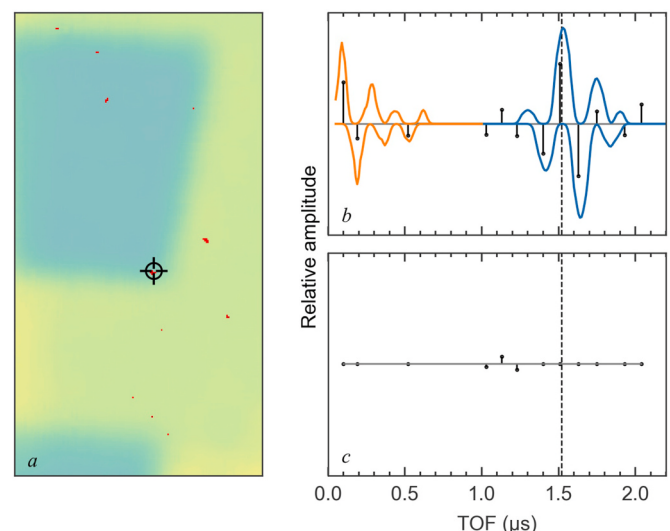


Fig. 9. Subtraction of the reconstructed reference in presence of an indication.

thicknesses ranging from 1.70 to 5.68 mm. Various outer layers are used to consider the effect of different surface finishes commonly met in aerospace (see Table 1 for details). A total of 773 artificial defects were inserted in the test panels. The defects are circular with diameters ranging from 3.2 to 12.7 mm. Different materials are used: Teflon tape inserts simulating delamination and diverse foreign object debris (FOD) usually found in a context of production such as peel ply, bagging and release films. Defects are either inserted in flat regions of the panels (557 defects) or in ply drop-off areas (216 defects). They are distributed throughout the specimens' thickness, from first to last carbon ply.

The 13 RPB are actual parts inspected in production and were used to evaluate the overall analysis time and to verify the number of false positives, as they include no artificial defect.

For the aft fuselage skins (noted AFS from this point), 2 test specimens were used: one flat panel with different thickness steps and another one with 2 co-cured stringers. The specimens are monolithic unidirectional CFRP panels with thicknesses ranging from 1.28 to 9.56 mm (see Table 2). The same outer layers as for the bulkhead are considered. A total of 359 artificial defects were inserted in the test specimens. The defects are either circular with diameters of 6.4, 8.9 and 12.7 mm, or rectangular with width ranging from 3.8 to 12.7 mm and length from 8.5 to 12.7 mm. All artificial defects for these test panels are made of Teflon. They are either located in flat regions of the panels (300 defects) or in stringers areas (59 defects). They are also distributed in the part thickness, from 1st to last carbon ply. Eleven actual AFS were also used to evaluate the number of false positives and to measure the analysis duration.

The specimens were inspected using an automated gantry system and 5 MHz phased-array probes put in contact with the components by means of a water box. A-scans were collected using the pulse-echo technique. The pitch of the linear array is 1 mm and a 4 elements active aperture was formed and electronically shifted across the probe axis by steps of 1 element. As the probe was moved, A-scans were recorded at every millimeter in the scan direction generating 1 mm × 1 mm pixels C-scans. The data collected for each part was then analyzed using the program developed in Ultis® and the different additional tools described in Sections 2.2 to 2.4.

ToF C-scans of remaining indications were obtained using either BWEF, the new proposed algorithm or a combination of both (using binary addition). Both methods parameters were optimized using the following procedure.

The same criterion on the maximum acceptable number of false calls was used for both the BWEF tool and the new method. A maximum of 50 false positives per part was defined as reasonable for a first deployment in production, based on the time required by an operator to analyze a false call (i.e., examining the corresponding A-scan signal). The threshold of the detection gate applied to the A-scan and the BWEF tool parameters were set to minimize the false call rate on the 13 RPB and 11 AFS components available for the study while maximizing the detection on the flat test panels. A similar optimization process was used for the new algorithm. The false calls results are discussed in Section 4.

L_{MAX} was defined as the largest dimension of an indication (in mm), W_{MAX} as its widest dimension in the direction perpendicular to L_{MAX} (in

Table 1
Test panels used for the rear pressure bulkhead.

Test specimens characteristics	
Thickness steps	From 1.70 to 5.68 mm (6 different steps)
Outer layers	Carbon ply/Glass ply/Copper mesh
Zones	Flat areas/Ply drop-offs
Artificial defects characteristics	
Shape	Circular
Diameters	3.2/3.8/5.1/6.4/8.9/9.5/9.7/12.7 mm
Materials	Teflon/Peel ply/Bagging/Release film
Depth	From first to last ply

Table 2

Test panels used for the aft fuselage skins.

Test specimens characteristics	
Thickness steps	From 1.28 to 9.56 mm (28 different steps)
Outer layers	Carbon ply/Glass ply/Copper mesh
Zones	Flat areas/Stringer regions
Artificial defects characteristics	
Shape	Circular or rectangular
Diameters of circular inserts	6.4/8.9/12.7 mm
Widths of rectangular inserts	3.8/5.1/8.5/8.9/12.7 mm
Lengths of rectangular inserts	8.5/8.9/12.7 mm
Materials	Teflon
Depth	From first to last ply

mm) and S as the indication area (in mm²). Two different sets of detection criteria were used depending on the considered region, in order to limit the number of false positives. For flat portions of the panels, an indication is detected if $L_{MAX} \geq 3$ mm or $W_{MAX} \geq 3$ mm or $S \geq 9$ mm². In the ply drop-off regions, the detection criteria are $L_{MAX} \geq 4$ mm or $W_{MAX} \geq 4$ mm or $S \geq 16$ mm². These detection criteria (minimum defect length, width and surfaces) were applied to each C-scan and a hit and miss table was produced for each method.

A probability of detection (POD) approach based on the likelihood ratio method [15,16] was used for the RPB to compute the overall $a_{90/95}$ values, i.e., the defect size that can be detected at 90% probability with a confidence interval of 95%. Detected percentages (number of "hits" divided by total number of defects) were also calculated for three depth categories: shallow (between 1st and 2nd carbon ply), inner (from 2nd to penultimate carbon ply) and deep defects (between penultimate and last carbon ply). Different subsets of data were also analyzed to study the influence of the considered region in the AFS (stringers or skin areas).

4. Results and discussion

4.1. Results for the RPB

The overall number of false positives was evaluated on the 13 RPB and was found to be acceptable (max. 50 per part) for most of the scans. However, a minority of components exhibited more than 50 false calls for both the BWEF and the new algorithm, even with the optimized detection parameters. These indications were analyzed using the A-scan signals and were then distributed among different causes: local coupling issues, error in the synchronization of the A-scan causing a shift of the first peak, presence of pre-drilled holes on the part. Most of these causes are linked to hardware or software aspects of the inspection gantry used during the study. This equipment is an existing production machine that was not specifically designed nor optimized for automated analysis. Solutions to the listed issues are well known and could be easily implemented if the automated analysis methods were to be deployed in production. The number of false calls should then be drastically reduced. However, the required adjustments could not be made during the present study as this inspection equipment was already used in production (without automated analysis). The optimized detection parameters generating less than 50 false positives for most components were thus validated for the current study.

POD curves for each of the 3 defect extraction methods are presented on Fig. 10. The differences observed in the detection percentage depending on defect depth (shallow, inner or deep defects) are shown on Fig. 11.

The resulting $a_{90/95}$ obtained with the developed method is 13.4 mm if the defect detection is applied on C-scans processed with the BWEF, 8.3 mm with C-scans processed with the new algorithm and 6.8 mm with C-scans combining the results of both algorithms (Fig. 10). The overall performance is thus significantly better if the new defect extraction approach is used in parallel or in complement of the BWEF. A more detailed analysis (Fig. 11)

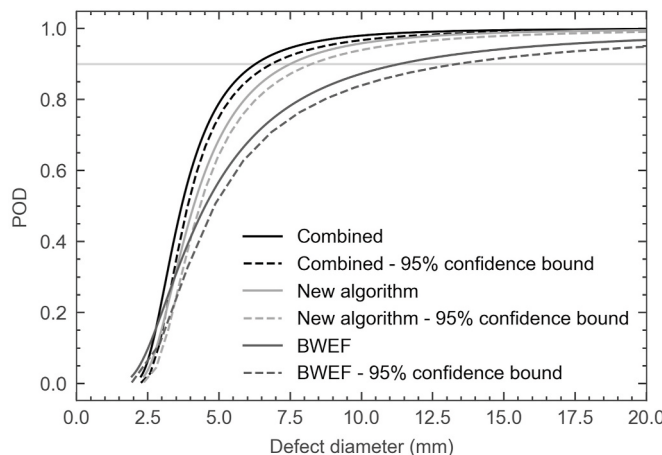


Fig. 10. POD curves for 3 defect extraction methods: BWEF, new algorithm, and combined results.

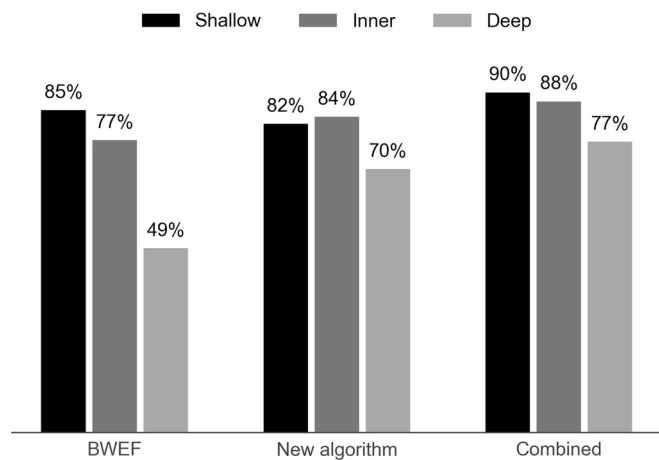


Fig. 11. Detection results vs depth of defects for the BWEF, the new algorithm and combination of both.

shows that detection percentages are especially higher with the new algorithm for deep defects. These defects are very close to the backwall surface, considering the low ply thickness of the RPB (approx. 0.150 mm), and are thus more likely to be suppressed by the BWEF, which detects only 49% of *deep* defects. The new algorithm appears more adapted for these defects: 70% of *deep* defects are detected.

However, the BWEF detects some defects missed by the new algorithm, especially *shallow* defects. This may be caused by the entry echo reference envelopes calculated by the new algorithm that had to be enlarged to reduce the number of false positives. Indeed, we observed that most of the false positives appear just after the entry echo, mainly caused by the issues listed in the first paragraph of the present section. The reference envelopes calculation takes this effect into account to limit the false calls in this region of the A-scan, the downside being the loss of some *shallow* defects.

The *combined* results obtained by binary addition lead to the best overall detection performance, as shown on Figs. 10 and 11. However, it is worth noting that although binary addition increases the number of detected defects, it might also increase the number of false positives. The new algorithm brings the most benefits for *inner* and, more significantly, for *deep* defects. Since most false positives come from peaks close to the entry echo (in the *shallow* zone), the method should be optimized by using BWEF only for the shallowest depths and the new method for the deeper ones. Applying each algorithm to a different depth range should prevent the potential addition of false calls and will be considered as a

future development of the method. A proper evaluation of the achievable false call rate will then be conducted with corrected inspection factors (especially concerning the issues previously listed in this section) and the improved combination method.

Fig. 12 illustrates an example of C-scans obtained with the BWEF and the new algorithm for artificial defects made of three different materials (peel ply, Teflon and bagging film) located in a ply drop-off region. In this example, the new detection method is able to generate more accurate representations of the defects, especially for the weakest acoustic reflectors (peel ply and bagging film).

Finally, the analysis time measured for a full RPB was found to be approximately reduced by a factor of 3 compared to the current analysis performed by human operators.

4.2. Results for the AFS

For the AFS panels, the larger size of inserts, and more favorable materials and locations (discussed later in this section) resulted in only one miss in the skin area. Furthermore, the number of defects embedded in the stringers regions was too low [15,17]. For the foregoing reasons, classic POD curves could not be evaluated. Table 3 shows the number of defects detected in AFS test panels with the method described in this paper and for the three possible defect extraction approaches: BWEF, new algorithm and combination of both.

The detection methods give very high detection rates on AFS test panels, especially in the skins areas: 299/300 artificial defects are detected by the BWEF and 300/300 by the new algorithm. In stringers areas, the combined method has the best performance (58/59, i.e., 98%), underlining the complementarity of both approaches which individually exhibit excellent detection percentages of respectively 92% (54/59) for the BWEF and 88% (52/59) for the new algorithm.

Two elements explain the gap observed between RPB and AFS detection results. First, the AFS test panels only include Teflon inserts, whereas RPB panels contain 44% of FOD (peel ply, bagging film or release film) and 56% of Teflon. Teflon inserts are stronger acoustic reflectors than FOD and are thus more easily detected. Secondly, the previous section showed that the new algorithm yields better detection results for *deep* defects, but has similar performance for the other defect depths. However, the proportion of *deep* defects in AFS test panels is lower than in RPB (10/59 in stringers areas and 64/300 in skins for AFS, compared to 234/773 in the RPB test panels).

These two reasons make RPB test panels much more challenging than AFS panels and explain the large difference observed in the detection results.

Fig. 13 illustrates the results obtained on a portion of an actual AFS containing artificial defects. Such area can be analyzed in all its complexity through the segmentation approach that was developed. Fig. 13 shows that the new algorithm is able to detect more defects than the BWEF in this

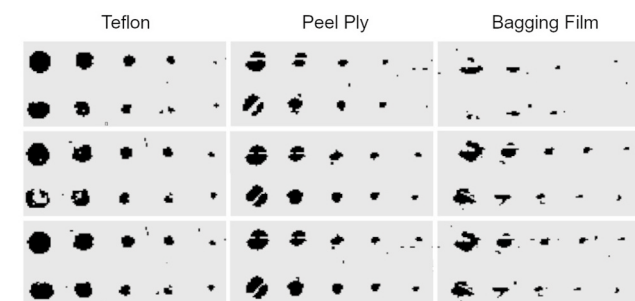


Fig. 12. Example of C-scans obtained in a ply drop-off area for different defects materials with (a) BWEF, (b) the new detection algorithm and (c) the combined method.

Table 3
Defect detection in AFS test panels.

	Skins	Stringers
Total number of defects	300	59
BWEF	299	54
New algorithm	300	52
Combined	300	58

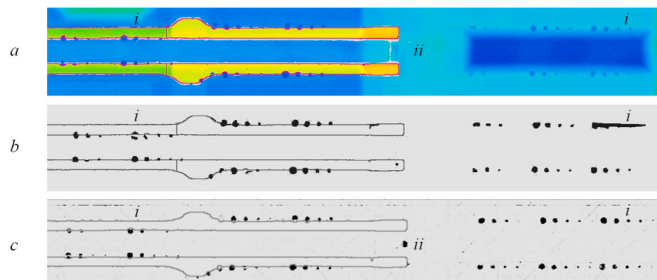


Fig. 13. Example of C-scans obtained on an actual AFS in an area including a stringer and thickness variations: images are the original ToF C-scan (a) and the C-scans processed by the BWEF (b) and by the new algorithm (c).

particular area, and to give better representations of the defects (as shown in areas indicated by *i*). The defect *ii* is a circular Teflon insert of diameter 12.7 mm located in the stringer run-out. Thickness variations due to the manufacturing process always occur in this area and make defects particularly difficult to detect with the BWEF. The new algorithm was able to detect this defect.

Finally, based on the tests done on the 2 actual AFS, the total analysis duration should be reduced by a factor of approximately 5 compared to the current method.

5. Conclusions

A method was developed for the automated analysis of ultrasonic data applied to the aft fuselage components of a passenger aircraft. The method is based on Ultis® existing features complemented by new approaches and tools which involved a projection optimizer for the C-scans acquired in 3D, an efficient segmentation method and a new defect detection algorithm. Performance evaluation was conducted using flat test panels including artificial defects as well as actual parts. The results show that the method is able to process large and complex components, from the loading of the 3D data file to the generation of inspection reports and allows for significant time savings compared to visual analysis. The segmentation approach allows for the analysis of the entirety of complex parts including co-cured stringers, ply drop-offs, uncontrolled thickness changes, holes and edges. The new detection algorithm gives better results than Ultis® native tools for defects close to the backwall surface, especially in the case of thin carbon plies, and generates more accurate images of weak acoustic reflectors located in steep thickness variations. Used in conjunction with Ultis®, this algorithm can achieve excellent detection performance in every area of a complex component, provided that both methods are combined in a way that limits the number of false positives generated.

CRediT authorship contribution statement

Loïc Séguin-Charbonneau: Conceptualization, Methodology, Formal analysis, Software, Writing – original draft, Visualization. **Julien Walter:** Conceptualization, Methodology, Formal analysis, Validation, Writing – review & editing, Project administration, Funding acquisition. **Louis-Daniel Théroux:** Methodology, Formal analysis, Validation, Visualization. **Laurent Scheid:** Methodology, Formal analysis, Validation, Visualization. **Alexandre Beausoleil:** Data curation. **Benoit**

Masson: Conceptualization, Methodology, Investigation, Resources.

Declaration of competing interest

The authors declare that they have no known competing financial interests or personal relationships that could have appeared to influence the work reported in this paper.

Acknowledgements

This work was supported by the Natural Sciences and Engineering Research Council of Canada (NSERC), Fonds de recherche du Québec - Nature et technologies (FRQNT), Bombardier Aviation and the Programme d'aide à la diffusion des résultats de recherche au collégial (PADRRC) of Québec's Ministère de l'Enseignement supérieur (MES). Computing resources were provided by Compute Ontario, Calcul Québec and Compute Canada. The authors would like to thank Tomy Brouillette and Olivier Arès from Centre technologique en aérospatiale for their valuable help with data analysis and POD study.

References

- [1] Workman GL, Kishoni D, Moore PO. Ultrasonic testing, Nondestructive testing handbook, third ed., vol. 7. Columbus, OH: American Society for Nondestructive Testing; 2007. ISBN 978-1-57117-105-4 1-57117-105-3.
- [2] Bossi RH. American Society for Nondestructive Testing., ASNT industry handbook : aerospace NDT. Columbus, OH: American Society for Nondestructive Testing; 2014. ISBN 978-1-57117-339-3 1-57117-339-0.
- [3] Aldrin JC, Coughlin C, Forsyth DS, Welter JT. Progress on the development of automated data analysis algorithms and software for ultrasonic inspection of composites. AIP Conf Proc 2014;1581(1). <https://doi.org/10.1063/1.4865058>. 1920–1927, ISSN 0094-243X.
- [4] Mahmud MF, Pauzi MZM, Bakar EA. Flatbed scanner image and single ultrasonic rangefinder technique for composite laminates defect detection. 2013 IEEE Int Conf on Smart Instrum, Meas and Appl (ICSIMA) 2013:1–5. <https://doi.org/10.1109/ICSIAMA.2013.6717929>.
- [5] Goodfriend L. Automatic processing of ultrasound images for nondestructive testing. In: Braggins DW, editor. Comput Vis for Ind, vol. 1989. SPIE: International Society for Optics and Photonics; 1993. p. 173–82. <https://doi.org/10.1117/12.164859>.
- [6] Smith RA, Nelson LJ, Mienczakowski MJ, Challis RE. Automated analysis and advanced defect characterisation from ultrasonic scans of composites. Insight - Non-Destr Test and Cond Monit 2009;51(2):82–7. <https://doi.org/10.1784/insi.2009.51.2.82>.
- [7] Pérez C, Fernández F, Borrás M. Automatic analysis of UT inspections in aircraft structures (MIDAS-AUTODET software). ECNDT; 2006.
- [8] Simas Filho EF, Souza YN, Lopes JLS, Farias CTT, Albuquerque MCS. Decision support system for ultrasonic inspection of fiber metal laminates using statistical signal processing and neural networks. Ultrasonics 2013;53(6):1104–11. <https://doi.org/10.1016/j.ultras.2013.02.005>. ISSN 0041-624X.
- [9] Barut S, Dominguez N. NDT diagnosis automation: a key to efficient production in the aeronautic industry. In: Proc of the 19th World Conf on non-Destr test (WCNDT 2016), Munich, Germany; 2016. URL, <https://www.ndt.net/search/docs.php?3?id=19184>.
- [10] Rieder H, Salzburger H-J. Alok-imaging and -reconstruction of surface defects on heavy plates with E.M.A.-Rayleigh wave transducers. In: Thompson DO, Chimenti DE, editors. Review of progress in Quantitative nondestructive evaluation: volume 8, Part A and B. Boston, MA: Springer US; 1989. https://doi.org/10.1007/978-1-4613-0817-1_142. 978-1-4613-0817-1, 1127–1135.
- [11] Séguin-Charbonneau L, Walter J, Masson B. A novel automatic defect detection method for the ultrasonic inspection of aircraft composite parts. In: 46th Annu Rev of Prog in Quant nondestruct evalution. Portland, OR: Iowa State University Digital Press; 2019. URL, <https://www.iastatedigitalpress.com/qnde/article/id/8601/>.
- [12] Golub GH, Reinsch C. Singular value decomposition and least squares solutions. In: Wilkinson JH, Reinsch C, Bauer FL, editors. Linear Algebra, Handbook for automatic computation. Berlin, Heidelberg: Springer; 1971. https://doi.org/10.1007/978-3-662-39778-7_10. 978-3-662-39778-7, 134–151.
- [13] Powell MJD. An efficient method for finding the minimum of a function of several variables without calculating derivatives. Comput J 1964;7(2). <https://doi.org/10.1093/comjnl/7.2.155>. 155–162, ISSN 0010-4620.
- [14] Dierckx P. Curve and surface fitting with splines. USA: Oxford University Press, Inc.; 1993. ISBN 978-0-19-853441-9.
- [15] MIL-HDBK-1823A, Nondestructive evaluation system reliability assessment, Department of Defense Handbook .
- [16] Kendall MG, Stuart A. The advanced theory of statistics. second ed., vol. 2. New York: Inference and Relationship, Hafner; 1967.
- [17] Annis C, Gandossi L, Martin O. Optimal sample size for probability of detection curves. Nucl Eng Des 2013;262:98–105.

Loïc Séguin-Charbonneau is a physics professor at Cégep Édouard-Montpetit and a researcher at Centre technologique en aérospatiale. He specializes in mathematical optimization and modeling of physical systems. Over the last few years, he did research in network optimization, scheduling optimization, stellar astrophysics and ultrasound testing

Julien Walter is head of NDT department at Centre technologique en aérospatiale since 2013. Before joining CTA, he had worked as an R&D engineer for 10 years, mainly in the field of industrial and medical applications of ultrasound. His research interests include phased-array probes design, advanced NDT techniques development and ultrasonic data analysis

Louis-Daniel Théroux is a physics engineer at Centre technologique en aérospatiale. Although his main expertise is in thermography, he also has experience in several other non-destructive methods such as ultrasound and shearography. He is specialized in the study of heat transfer, the characterization of thermal properties and the application of non-destructive methods on composite materials.

Laurent Scheid is a professor of aerospace engineering at Cégep Édouard-Montpetit and a researcher at Centre technologique en aérospatiale. His field of work includes several non-destructive techniques such as ultrasound and bondtesting. Over the last few years, he contributed to research projects concerning the inspection of composite materials in aerospace, for both in-service and manufacturing applications.

Alexandre Beausoleil is a physics professor at Cégep Édouard-Montpetit and a researcher at Centre technologique en aérospatiale. He specializes in mathematical optimization and modeling of physical systems. He recently worked on thin film growth modeling and non-destructive testing, including probability of detection, heat transfer and ultrasonic inspection.

Benoit Masson is a specialist in ultrasonic inspection, certified ASNT UT 3 and NAS410 UT 3. He works in the Material & Process engineering group of Bombardier Aviation and has more than 12 years of experience in aerospace industry. He works mostly in development of ultrasonic inspection techniques in service and approbation of ultrasonic process in production for Bombardier manufacturing plants and suppliers.